The FliI ATPase couples ATP hydrolysis to substrate switching in bacterial flagellar type-III secretion

Rosa Einenkel[a], Mario Delgadillo-Guevara[a,b], Lasse Hallenga[a], Christian Goosmann[c], and Marc Erhardt[a,d]#

[a]Humboldt-Universität zu Berlin, Institute of Biology, 10115 Berlin, Germany

[b]Department of Biochemistry and Pharmacology, Bio21 Molecular Science and Biotechnology Institute, The University of Melbourne, Melbourne, VIC, Australia

[c]Max Planck Institute for Infection Biology, 10117 Berlin, Germany

[d]Max Planck Unit for the Science of Pathogens, 10117 Berlin, Germany

Running Head: FliI ATPase Controls Flagellar Secretion Specificity

#Correspondence to: marc.erhardt@hu-berlin.de

Word count abstract: 159

Word count significance: 119

Word count text: 6655

Abstract:

Bacterial flagella are assembled by a specialized type III secretion system that exports structural subunits in a defined order. While the ATPase FliI is known to couple ATP hydrolysis to substrate translocation, its role in the transition between early and late secretion stages has remained unclear. Here, we systematically analyzed *Salmonella enterica* strains with defined FliI point mutations and found that FliI activity is dispensable for early substrate export and hook-basal body formation but is important for triggering the substrate specificity switch and promoting late substrate export. Mutant strains showed delayed gene expression from class 3 promoters, prolonged early secretion, and impaired flagellar filament assembly, despite normal FliI localization and oligomerization. These findings support the involvement of FliI in controlling the temporal dynamics of flagellar assembly. We propose that FliI contributes to substrate switching, ensuring robust and orderly fT3SS function. This study highlights the multifaceted role of the fT3SS ATPase in optimizing the efficiency and robustness of flagellum assembly.

36 **Significance:**

37 The ordered export of substrates by bacterial type III secretion systems is essential for
38 the assembly of complex surface structures such as the flagellum, yet the mechanisms
39 that control the timing of substrate switching remain poorly understood. The bacterial
40 flagellar ATPase FliI is best known for being involved in energizing the flagellar type III
41 secretion system. Here, we show that FliI contributes to the transition from early to late
42 substrate export during flagellar biogenesis. Using targeted FliI mutants in *Salmonella*,
43 we show that ATPase activity is dispensable for early export but important for proper
44 substrate switching and late-stage flagellar assembly. These findings highlight the
45 multifaceted roles of FliI during flagellar assembly beyond activating the flagellar type III
46 secretion system.

Introduction:

Bacterial flagella are complex nanomachines that play a crucial role in motility, enabling bacteria to navigate through their environment (1). This motility is essential for many bacterial processes, including colonization and adhesion to host cells (2). The flagellum consists of three major structural components: the basal body, the hook and the filament (**Fig. 1A**). The basal body (BB) anchors the flagellum to the bacterial cell envelope and serves as the motor apparatus, generating the rotational force that drives motility (3, 4). It is composed of several ring-like structures, including the peptidoglycan-spanning P-ring the outer membrane L-ring and the inner membrane MS-ring, which connects to the rotor (3, 4). The rotor, or C-ring links the flagella mediated motility to the process of chemotaxis and acts as the rotary switch complex (5-7). The stator units generate the rotational force that drives the rotation of the C-ring and hence the flagellar filament (8). The proximal rod and the distal rod form the secretion channel through the cell envelope. The hook acts as a flexible joint between the BB and the filament (9), with its length precisely regulated (10, 11). The hook-filament junction connects the hook to the filament, which consists of tens of thousands of subunits of a single protein, the flagellin (either FliC or FljB in *S. enterica*) and acts as a mechanical buffer zone to smoothly connect the flexible hook and the rigid filament (12). The filament's distal end is capped by a pentamer of FliD, a specialized structure, that facilitates the assembly of flagellin subunits into a functional filament (12, 13).

The secretion of axial proteins is tightly regulated and mediated by the flagellar type III secretion system (fT3SS), which is responsible for the translocation of most extra-cytoplasmic flagellar components from the bacterial cytoplasm to the site of assembly, a

70 process that is mainly powered by the proton motive force (14). The fT3SS as part of the
71 BB consists of the membrane embedded export gate (FlhA, FlhB) and secretion pore
72 (FliP, FliQ and FliR), as well as a cytoplasmic ATPase complex (FliH, FliI and FliJ) (15).
73 FliI, a Walker-type AAA^+-ATPase with two highly conserved motifs for nucleotide binding
74 (Walker A) and ATP hydrolysis (Walker B), forms a hexameric ring structure at the base
75 of the flagellum with FliJ as the central stalk, anchored to the basal body by 12 FliH
76 molecules through interactions with the motor protein FliN (16-21). The ATPase complex
77 is thought to couple ATP hydrolysis to the activation of the export gate through
78 interactions of FliJ with the export gate protein FlhA to ensure efficient and robust protein
79 export (22). While a previous study had proposed a potential interaction between the
80 second messenger c-di-GMP and the fT3SS ATPase FliI (23), the exact role of this
81 interaction remains unclear. Furthermore, heterotrimers of 2 FliH and 1 FliI are thought to
82 play an important role in the dynamic delivery of substrates to the export gate, ensuring
83 the timely assembly of the flagellar components (24). Based on the known functions of
84 the evolutionarily related ATPase InvC from the virulence-associated T3SS, as well as
85 insights from mathematical modeling, FliI has been proposed to play roles in substrate
86 unfolding and in dissociating substrates from their cognate chaperones (25, 26).
87 However, although extensively studied, the exact molecular mechanisms of the fT3SS
88 ATPase complex remain incompletely understood (27).

89 Flagellum biogenesis and flagellar gene expression are tightly regulated through
90 a hierarchical system to ensure proper assembly and efficient energy utilization. This
91 process involves three distinct classes of promoters, starting from the class 1 promoter
92 that drives the expression of the master regulator $FlhD_4C_2$. $FlhD_4C_2$ activates expression

93 from class 2 promoters, that encode structural components of the hook-basal body (HBB)
94 as well as regulatory proteins like the flagellar-specific transcription factor σ^{28} and its anti-
95 σ factor FlgM. FlgM coordinates the temporal progression of flagellar gene expression by
96 sequestering σ^{28}, thereby inhibiting transcription from class 3 promoters until hook
97 assembly is completed. Hook completion acts as a checkpoint that signals the export
98 apparatus to switch substrate specificity from early substrates (rod and hook components)
99 to late substrates (filament components). This transition, mediated by FlhB and FliK,
100 ensures proper hook length, which is essential for optimal motility and flagellar bundle
101 formation (10, 11, 26). Late substrates require chaperones for their efficient export and to
102 prevent premature interactions and degradation. Upon the substrate specificity switch,
103 FlgM is recognized as a late substrate and secreted via the fT3SS, freeing σ^{28} to finally
104 initiate transcription from class 3 promoters, thereby elegantly connecting proper
105 flagellum assembly with gene regulation (25, 28, 29). Genes expressed from class 3
106 promoters encode, among others, the flagellins, the stator units and key components of
107 the chemotaxis system (30).

108 In this study, we dissected the role of the flagellar ATPase FliI by generating
109 targeted point mutations in its ATPase domain and adjacent regions implicated in
110 secretion control. Through a combination of mutagenesis and functional assays, we
111 identified mutants that exhibited selective defects in the secretion of late substrates and
112 in the substrate specificity switch, while early substrate export and hook assembly
113 remained unaffected. These results demonstrate that FliI is dispensable for early stages
114 of flagellar assembly but important for triggering the transition to late-stage export. Our
115 findings support a model in which FliI not only powers secretion via ATP hydrolysis but

116 also actively supports the substrate switching mechanism, thereby ensuring the temporal

117 fidelity and efficiency of flagellar biogenesis.

118 **Results**:

119 The Walker-type AAA+ ATPase FliI from *S. enterica* plays a crucial role in flagellar
120 assembly by ensuring a robust export of substrates through the fT3SS. To investigate the
121 molecular function of FliI, we generated point mutations at residues implicated in its
122 catalytic activity and putative regulatory sites (23, 31). All mutations were introduced into
123 the *S. enterica* genome to maintain native expression conditions. Specifically, we created
124 mutations at residues located at the interface between FliI monomers (R177H and
125 E215Q), and in the nucleotide-binding Walker A motif within the central cavity of the FliI
126 hexamer (G183A). Additionally, E215 was previously shown to be involved in the catalytic
127 activity of FliI (19). We included two previously characterized Walker B mutants (E211D
128 and E211Q), known to drastically reduce ATPase activity - by 100-fold and completely,
129 respectively - resulting in impaired motility and substrate secretion (31).

130 The effect of *fliI* point mutations on swimming motility was assessed using a soft-agar
131 motility assay (**Fig. 1B-C**). As anticipated, the *fliI* deletion mutant (Δ*fliI*) was non-motile,
132 consistent with previous reports (14). The R177H mutant displayed 48% motility, while
133 the E215Q mutant was non-motile. The Walker A motif mutant G183A exhibited a slight
134 reduction in motility to 93% of the WT level. The Walker B motif mutants E211D and
135 E211Q showed 25% motility or loss of motility, respectively. These phenotypes suggest
136 defects in flagellar assembly, prompting further investigation into how these specific
137 mutations impair motility.

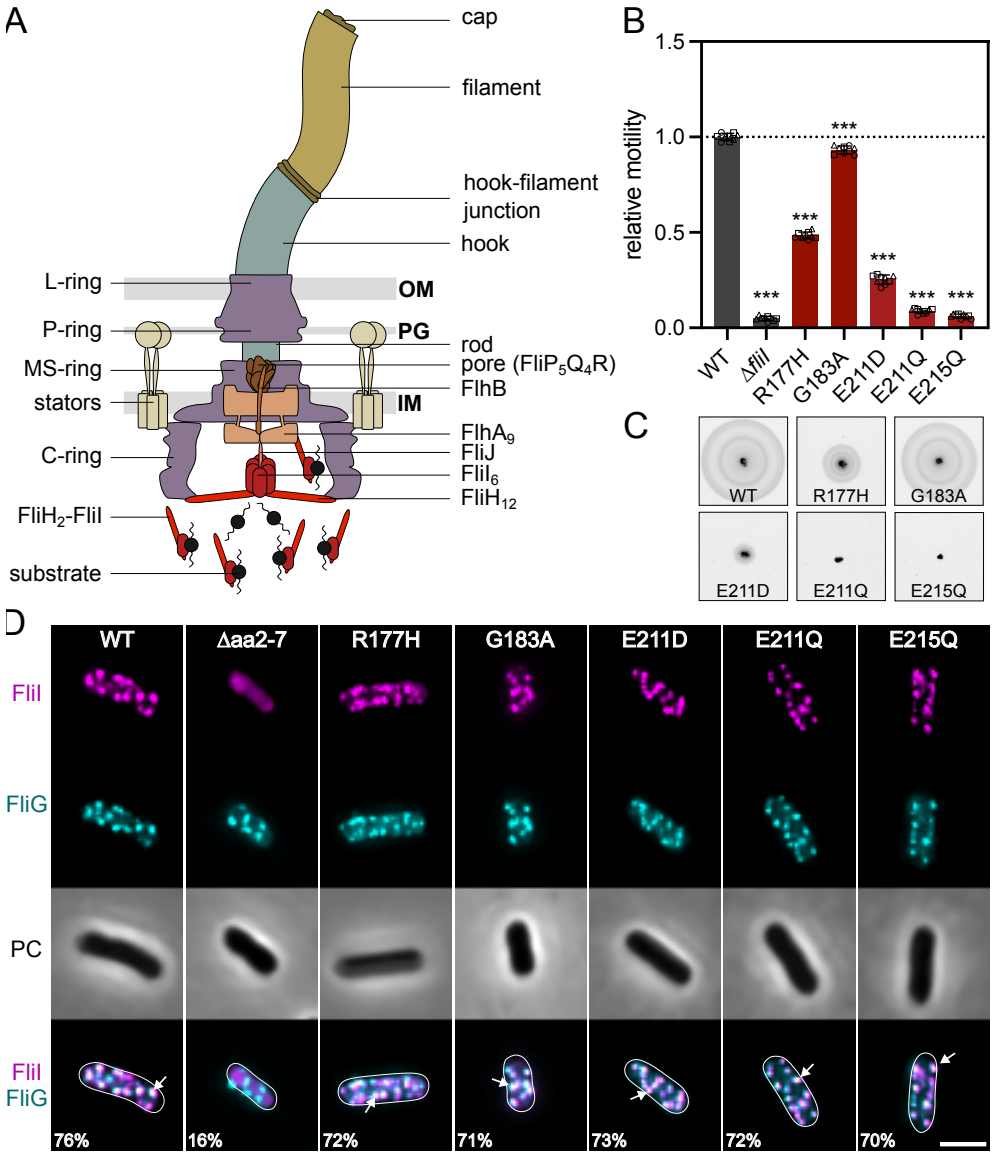

Fig. 1 FliI is required for flagellar motility and efficient assembly of the flagellar export apparatus. (A) Schematic of a gram-negative bacterial flagellum and the flagellar type III secretion system (fT3SS). The flagellar motor spans the inner membrane (IM), periplasmic space including the peptidoglycan (PG), and outer membrane (OM), and assembles an external filament via a central secretion channel. The cytoplasmic ATPase complex (FliHIJ) delivers substrates and activates the export gate through ATP hydrolysis. (B) Relative motility of wildtype (WT) and *fliI* mutants analyzed using soft-agar motility plates, quantified after 4-5 h incubation at 37 °C. Diameters of the motility halos were measured using Fiji and normalized to the WT. Bar graphs represent the mean of at least 3 biological replicates with standard deviation error bars. Replicates shown as individual data points. ***$p < 0.001$ (ordinary one-way ANOVA with Dunnett's multiple comparison test vs. WT). (C) Representative swimming halos of the WT and *fliI* point mutants. (D) Representative microscopy images of WT and *fliI* mutants. FliI-HaloTag labeled with TMR-ligand (magenta), basal bodies visualized with mNeonGreen-FliG (cyan); PC (PhaseContrast). Percentage of FliI-FliG foci pairs below the colocalization threshold (2 px) is indicated for each strain. White arrows show examples of colocalized foci. Scale-bar: 2 µm.

153 To investigate whether the phenotypes observed in the FliI mutants were caused by
154 subcellular mislocalization of the ATPase, we performed *in vivo* fluorescence microscopy.
155 In order to observe FliI localization, we constructed strains expressing FliI with a C-
156 terminal HaloTag fusion. To assess colocalization of the ATPase with the basal body, the
157 strains also expressed the C-ring component FliG with an N-terminal mNeonGreen
158 fusion. Flagellar biosynthesis was synchronized by replacing the native promoter of the
159 *flhDC* master regulator operon with an anhydrotetracycline (AnTc) inducible P_{tetA}
160 promoter (32). FliI-HaloTag was labeled with the cell-permeant ligand
161 tetramethylrhodamine (TMR), and fluorescence microscopy was performed on live cells
162 (**Fig. 1D**). We then quantified the spatial colocalization between foci detected in the
163 respective fluorescence channels by calculating pairwise distances between detected
164 spots across individual cells. Spots were considered colocalized if their distance was
165 below a predefined threshold (2 px or ~144 nm). The fraction of colocalized foci pairs was
166 calculated as the number of colocalized pairs divided by the total number of detected
167 pairs within a maximal distance (30 px or ~2µm).
168 In WT cells, FliI strongly colocalized with FliG at the basal body, forming distinct
169 overlapping foci with 76% of foci pairs below the colocalization threshold (**Fig. 1D**). As a
170 negative control, the FliI ∆aa2-7 mutant, which has been previously shown to be deficient
171 in hexamer formation (33) and interaction with FliH (34), displayed a diffuse cytoplasmic
172 localization, with no distinct FliI foci visible by microscopy. Due to the nature of the
173 analysis pipeline, which detects local intensity maxima, foci pairs were still found,
174 however only 16% were considered colocalized. This confirms that FliI ∆aa2-7 is unable
175 to localize to the basal body, likely due to its inability to properly form hexamers and

176 disrupted interaction with FliH. The FliI point mutants (R177H, G183A, E211D, E211Q,
177 E215Q) localized to the basal body similarly to the WT, as indicated by the presence of
178 discrete FliI foci (Figure 4D). The percentage of colocalized foci pairs was 72% for R177H,
179 71% for G183A, 73% for E211D, 72% for E211Q, and 70% for E215Q. These results
180 suggest that the FliI point mutations do not substantially impair the subcellular targeting
181 of FliI. Additionally, we confirmed that proper localization of FliI depends on FliH and FliN
182 but not on FliJ or FlhA, as previously reported (**Fig. S1A**) (21).

183 To assess whether the FliI point mutants affect hexamer formation, we performed *in vivo*
184 site-specific photo-crosslinking of FliI variants containing a photoactivatable pBpa residue
185 (FliI*) at the FliI-FliI interface (**Fig. S1B**). UV-dependent formation of higher molecular
186 weight FliI adducts was observed for WT FliI* and all its point mutants studied here,
187 indicating that these variants retain the ability to oligomerize (**Fig. S1C**). In contrast, FliI*
188 Δaa2-7 exhibited only a faint high molecular weight band, suggesting premature
189 oligomerization in the cytoplasm, likely due to the high-level plasmid expression of FliI*.
190 However, the reduced level of cross-links compared to the WT confirms that hexamer
191 formation in this mutant is defective but may still occur at low levels under the
192 experimental conditions. Taken together, these results demonstrate that while the
193 mutations in FliI impair motility to varying degrees, they do not substantially alter its
194 subcellular localization or ability to form oligomers. Thus, the observed motility defects in
195 the FliI point mutants may instead reflect disruptions in the secretion activity of the fT3SS.

196

197 **FliI facilitates secretion of late flagellar substrates**

198 The fT3SS mediates the assembly of the axial structures of the flagellum through two
199 distinct secretion modes: early and late. Upon hook completion, the fT3SS undergoes
200 conformational changes, allowing recognition and export of late substrates (11, 35). To
201 determine whether the motility defects of the FliI point mutants result from impaired
202 secretion, we systematically analyzed early and late substrate export in these strains.
203 First, we confirmed FliI localization in strains deleted for components that lock the fT3SS
204 in either the early (Δ*flgBC* (proximal rod), Δ*flgE* (hook)) or late (Δ*flgKL* (hook-filament
205 junction)) stages of flagellar assembly (**Fig. S1A**). Fluorescence microscopy revealed that
206 FliI colocalized with the basal body in both secretion states, indicating its presence at the
207 basal body throughout the flagellar assembly process. To analyze the secretion efficiency
208 of early substrates in FliI point mutants, we employed a hook protein / β-lactamase (FlgE-
209 Bla) reporter system (**Fig. 2A**) (36, 37). Deletion of the rod components FlgBC leads to
210 secretion of flagellar substrates into the periplasm (38), resulting in the ability to resist
211 ampicillin in correlation to the quantity of secreted FlgE-Bla. Therefore, we analyzed the
212 ability of the FliI mutants to grow in the presence of increasing ampicillin concentrations
213 and determined the concentration of ampicillin leading to inhibition of bacterial growth to
214 half of its maximum (IC_{50} [Amp], **Fig. S2A**) and then normalized it to WT levels (**Fig. 2B**).
215 A mutant lacking the MS-ring and therefore the entire fT3SS (Δ*fliF*), was used as a
216 negative control, representing the basal level of resistance against ampicillin (**Fig. S2A**).
217 Deletion of *fliI* resulted is a severe reduction of early substrate secretion to 2% of WT
218 levels, similar to the Δ*fliF* control strain (1%), consistent with previous observations (14).
219 Among the point mutants, G183A exhibited the highest secretion efficiency, with an IC_{50}

220 of 356 µg/mL corresponding to 138% of WT levels. The R177H mutant displayed
221 secretion comparable to WT (IC_{50} of 257 µg/mL compared to 256 µg/mL for WT), despite
222 reduced significantly motility. Thus, both R177H and G183A were proficient in early
223 substrate secretion, despite motility defects. In contrast, the ATPase activity mutants
224 showed impaired secretion. E215Q exhibited the most severe defect, with only 13% of
225 WT levels (32 µg/mL), though still 11-fold higher than the Δ*fliF* control. The Walker B motif
226 mutants E211D and E211Q retained partial secretion activity (62% and 37% of WT,
227 respectively). Importantly, this still represents a significant 52- and 31-fold increase of the
228 IC_{50} of the ATPase activity mutants E211D (IC_{50} = 157 µg/mL) and E211Q
229 (IC_{50} = 95 µg/mL) compared to the Δ*fliF* control strain, respectively (**Fig. S2A**).
230 For quantification of late substrate secretion, we next employed the Nano-Glo
231 extracellular detection system (Promega) and the split luciferase NanoBit (**Fig. 2A**) (39,
232 40). Strains were engineered to express late flagellar substrates translationally fused to
233 the small luciferase subunit HiBiT (41). Secreted HiBiT-tagged proteins accumulated in
234 the supernatant and were detected via luminescence (**Fig. 2C-F**).
235 All mutants with impaired early secretion (Δ*fliI*, E211D, E211Q, and E215Q) also exhibited
236 strong defects in the secretion of FlgM-HiBiT (**Fig. 2C**). Secretion levels were reduced to
237 0.1% (Δ*fliI*) , 0.4% (E215Q) , 0.7% (E211Q) and 7% (E211D) of WT levels. The R177H
238 mutant also showed a significant reduction (12.3%), while G183A retained 69.9% of WT
239 levels. FlgK-HiBiT secretion (**Fig. 2D**) was also reduced across all mutants. The strongest
240 defects were observed in *ΔfliI*, E215Q, and E211Q, each exhibiting less than 0.3% of WT
241 levels. E211D retained 8.2%, while R177H and G183A secreted 27.5% and 85.2% of WT
242 levels, respectively.

243 A similar pattern was observed for FliD-HiBiT (**Fig. 2E**), with secretion entirely abolished
244 in *ΔfliI*, E215Q, and E211Q (0.0%). E211D retained minimal export (1.8%), and secretion
245 was strongly to moderately reduced in R177H (19.6%) and G183A (60.5%).
246 E211D retained partial FliC-HiBiT (**Fig. 2F**) secretion (13.5% of WT), while the Δ*fliI* and
247 E215Q mutants showed only 0.1%, and E211Q 0.3% of WT levels. Secretion of FliC-
248 HiBiT was moderately reduced to 75.4% in G183A and more strongly in R177H (41.7%),
249 consistent with their motility phenotypes. Western blot analysis of cellular and secreted
250 fractions (**Fig. S2B–E**) confirmed the luminescence data. Additionally, reduced cellular
251 levels of FliC-HiBiT in most mutants suggested a delayed substrate specificity switch,
252 likely contributing to the impaired secretion phenotypes (**Fig. S2E**).
253 Secretion of all tested late substrates was consistently reduced across the *fliI*
254 mutants, suggesting a general requirement for FliI in late substrate export. Together,
255 these results are consistent with previous reports that early substrates can be secreted
256 with minimal ATP hydrolysis (31). The increased early substrate secretion in the G183A
257 mutant, and the unaffected secretion in the R177H mutant, indicate that FliI activity is
258 likely more critical for late substrate export than for early stages of assembly. This is
259 further supported by the observation that all ATPase activity mutants (E211D, E211Q and
260 E215Q) retained partial early secretion, despite strongly impaired ATPase activity.
261 Together, these findings suggest that FliI may promote late substrate export secretion
262 either by enhancing transport efficiency or by contributing to the substrate specificity
263 switch.

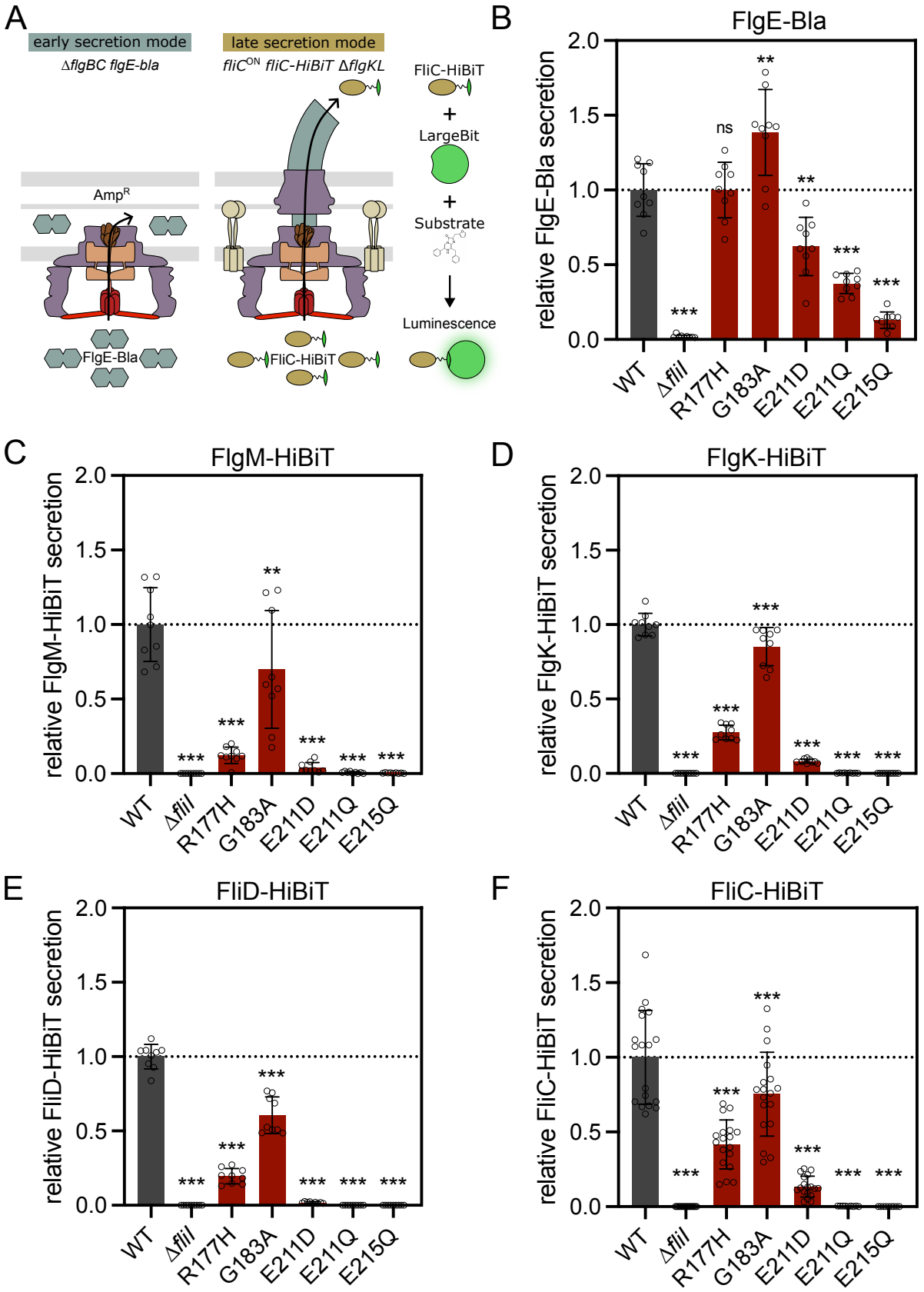
A
early secretion mode
ΔflgBC flgE-bla
late secretion mode
fliC^ON fliC-HiBiT ΔflgKL
AmpR
FlgE-Bla
FliC-HiBiT
FliC-HiBiT
+
LargeBit
+
Substrate
Luminescence
B
FlgE-Bla
relative FlgE-Bla secretion
C
FlgM-HiBiT
relative FlgM-HiBiT secretion
D
FlgK-HiBiT
relative FlgK-HiBiT secretion
E
FliD-HiBiT
relative FliD-HiBiT secretion
F
FliC-HiBiT
relative FliC-HiBiT secretion
WT
ΔfliI
R177H
G183A
E211D
E211Q
E215Q
ns
**
***

264

265 **Fig. 2** FliI facilitates secretion of late substrates. (A) Schematic of experimental set-ups to quantify secretion
266 of early (FlgE-Bla) and late substrates (example for FliC-HiBiT). Left: early substrate secretion was
267 measured in strains lacking proximal rod components, allowing secretion of FlgE-Bla into the periplasm,
268 where it confers ampicillin-resistance (Amp^R), proportional to the amount of secreted FlgE-Bla. Right: late
269 substrate secretion was quantified using the split Luciferase NanoBit. Strains were locked in FliC production
270 (*fliC*^{ON}) and lacked the hook-filament junction to prevent filament assembly (Δ*flgKL*). Cells expressed a
271 translational fusion of FliC to HiBiT. Addition of LargeBit and substrate to the culture supernatant enabled
272 luminescence detection proportional to secreted FliC-HiBiT levels. (B) Quantification of early substrate
273 (FlgE-Bla) secretion. Relative ampicillin resistance normalized to WT. Bars represent means ± SD from at
274 least 3 independent experiments; $^{**}p < 0.01$, $^{***}p < 0.001$; ns, not significant (ordinary one-way ANOVA
275 with Dunnett's multiple comparison test vs. WT). (C-F) Quantification of late substrate secretion, normalized
276 to the WT. Bars represent means ± SD from at least 3 independent experiments; $^{***}p < 0.001$ (ordinary
277 one-way ANOVA with Dunnett's multiple comparison test vs. WT).

278 **FliI contributes to the substrate specificity switch**

279 The observed decrease of late substrate secretion in the *fliI* mutant strains could have
280 resulted from either a defect in secretion efficiency of late substrates or from a defect or
281 delay in the substrate specificity switch. Before hook completion, the late substrate and
282 anti–σ^{28} factor FlgM inhibits the transcription of genes from class 3 promoters by
283 complexing the flagellar specific σ^{28} (42). The fT3SS undergoes a substrate specificity
284 switch upon complete formation of the HBB, which results in the secretion of FlgM,
285 thereby allowing formation of the σ^{28}-RNA-Polymerase holoenzyme and transcription
286 from class 3 promoters (43). Inefficient late substrate secretion would therefore not only
287 result in lower FliC secretion levels but simultaneously result in a lower abundance of late
288 substrates due to prolonged sequestration of σ^{28} by FlgM.

289 To address possible delays in the switch mechanism, gene expression from class 3
290 promoters was monitored using strains with an inducible *flhDC* master operon for
291 synchronized flagella formation and a plasmid harboring the reporter genes *luxCDABE*
292 under control of the class 3 promoter P_{motA} (44). We found for the WT a half-maximal
293 induction time of 93 ± 3 min of the P_{motA} promoter after *flhDC* induction (**Fig. 3A**, dotted
294 line). Further, the relative class 3 gene expression at T_{90} and T_{360} was determined (**Fig.
295 S2A**). The previously described slow hook polymerization mutant $flgE_{T149N}$ was utilized
296 as a control (45, 46). Since the hook polymerization in this mutant takes much longer, the
297 substrate specificity switch and therefore activation of transcription from class 3
298 promoters is delayed.

299 The G183A mutant displayed the mildest defect in the capability to perform the substrate
300 specificity switch with a relative class 3 gene expression of 78% and 85% at T_{90} and T_{360},
301 respectively. While P_{motA} showed only 18% of the WT activity at T_{90} in the R177H mutant,
302 the relative promoter activity reached 63% at T_{360}. The ATPase activity mutant E211D
303 showed a steady increase of relative class 3 gene expression over time, starting from 3%
304 at T_{90} to 71% at T_{360}. The E211Q mutant displayed a relative class 3 gene expression of
305 3% at T_{90} and T_{360}. In both Δ*fliI* and E215Q mutants the relative class 3 gene expression
306 stayed approximately the same over the course of the experiment, with 2% (T_{90}) and 1%
307 (T_{360}) relative expression observed. The *flgE*$_{T149N}$ mutant showed a delayed substrate
308 specificity switch, as expected, resulting in relative class 3 gene expression of 2% at T_{90}
309 and 11% at T_{360}.

310 A possible reason for the observed reduction of class 3 gene expression in the mutant
311 strains could be a reduced number of hooks. A slower hook polymerization, similar to the
312 *flgE*$_{T149N}$ control strain, and hence a reduced number of completed hooks would delay the
313 substrate specificity switch. Only upon completion of the HBB, the substrate specificity
314 switch occurs and the anti-σ28 factor FlgM will be recognized as a substrate of the fT3SS.
315 Accordingly, a delayed and/or decreased HBB formation frequency, resulting in FlgM
316 remaining inside the cell, would also explain the observed delay in class 3 gene
317 expression.

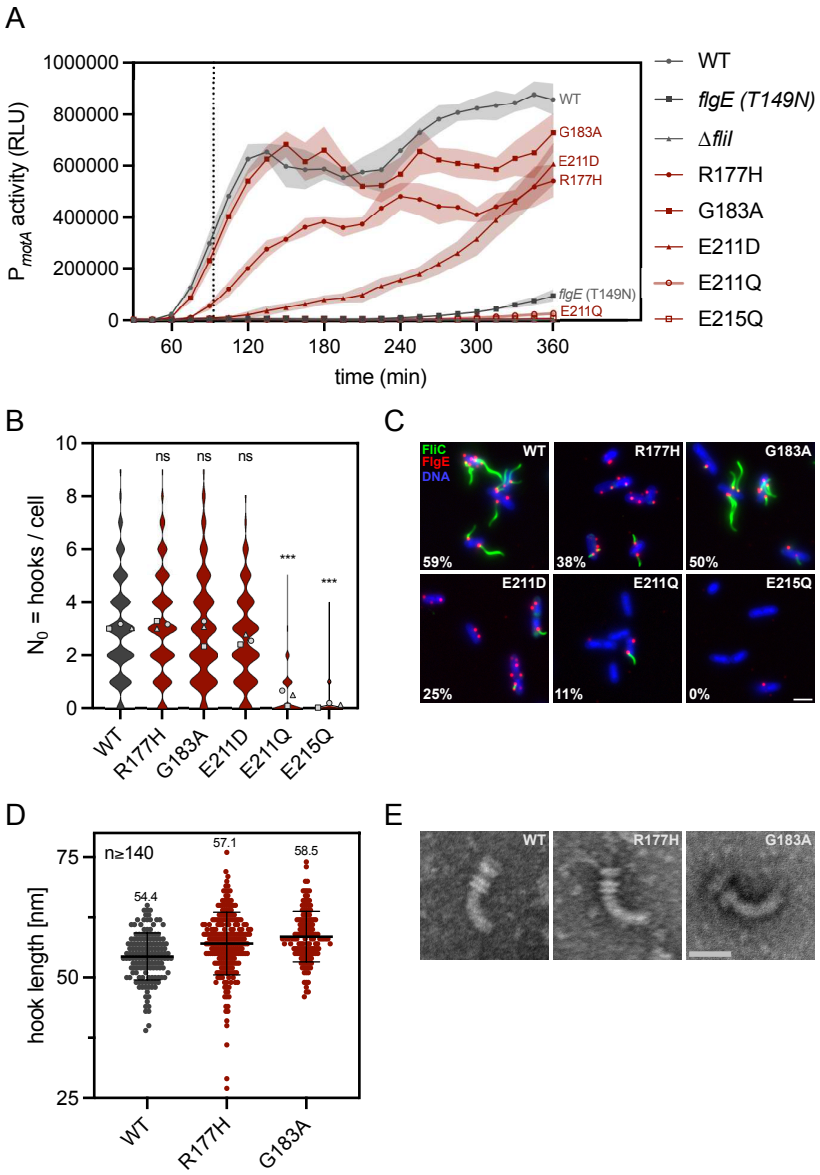

Fig. 3 FliI contributes to the substrate specificity switch. (A) Time course of P_{motA} activity (class III gene expression). Luciferase reporter activity was monitored in strains with synchronized flagella synthesis. Shown are the mean RLU (lines and symbols) ± SD (transparent lines) measured in 6 biological replicates. Dashed line indicates half-maximal induction time for P_{motA} in the wildtype (WT). (B) Quantification of hook number per cell determined by fluorescence microscopy. Violin plots represent distribution of the data from 3 biological replicates; symbols represent the mean of the biological replicates. ***$p < 0.001$; ns, not significant (ordinary one-way ANOVA on the means with Dunnett's multiple comparison test vs. WT). (C) Representative fluorescence microscopy images of WT and *fliI* point mutants. Filaments (FliC T237C) labeled with Star Green Maleimide (green), hooks ($FlgE_{3\times HA}$) immunostained with α-HA-Alexa555 (red) and DNA counterstained with DAPI. Percentage of hooks with an attached filament indicated in white. Scale-bar: 2 µm. (D) Hook length measurements from purified hook basal bodies. Symbols represent individual measurements, horizontal black line indicates mean ± SD error bars. (E) Representative negative-stain Transmission Electron Microscopy images of purified hook basal bodies. Scale bar = 50 nm.

332 To address this possible reason for the observed delayed substrate specificity
333 switch in the *fliI* mutants, we determined the number of hooks per cell (**Fig. 3B**). This was
334 especially interesting for the R177H and G183A mutant, since both mutants did not
335 display a reduction of early substrate secretion but showed reduced class 3 gene
336 expression levels (**Fig. 2C**, **Fig. 3A**). Furthermore, we determined the number of HBBs
337 with an attached filament (**Fig. 3C**, **Fig. S4**). We hypothesized, if the substrate specificity
338 switch was intact, that the ratio of attached filaments to the HBBs would be similar to the
339 WT. On the other hand, an increased number of HBBs without attached filaments would
340 suggest an impairment in the substrate specificity switch. To determine the number of
341 hooks and attached filaments per cell, we simultaneously visualized the hook and filament
342 using strains expressing $flgE_{3\times HA}$ for immunostaining of the hook and $fliC_{T237C}$ for
343 maleimide staining of the filament (**Fig. 3C**). In agreement to the early substrate secretion
344 levels, both R177H and G183A mutants did not show a difference in the amount of
345 assembled HBBs compared to the WT. The ATPase activity mutant E211D displayed a
346 slight, but non-significant reduction of hooks per cell. In contrast, E211Q displayed a
347 significantly reduced number of hooks with a maximum of five hooks per cell, compared
348 to nine in the WT. The number of cells without hooks just increased slightly from 8% (WT)
349 to 10% in E211D, whereas 55% of the E211Q mutant did not assemble any hooks. The
350 number of hooks per cell in the E215Q mutant only ranged from zero to four. However,
351 84% of the E215Q mutant cells did not assemble any hooks. Importantly, these findings
352 indicate that the reduced class 3 gene expression in the R177H and G183A mutants did
353 not result from a reduced number of hooks or slower hook polymerization. The reduced

354 number of hooks in the mutants E211Q and E215Q likely influenced the prolonged
355 suppression of class 3 gene expression.

356 The simultaneous hook and filament labelling also served for determining the percentage
357 of attached filaments per cell (**Fig. 3C**, **Fig. S4**). Therefore, filaments were counted on
358 previously analyzed cells with determined hook numbers. Since a filament can only be
359 assembled if the HBB formation is completed and the fT3SS has undergone the substrate
360 specificity switch, all cells without HBBs were excluded from this analysis. We therefore
361 reasoned that the frequency of filament formation, meaning the ratio of hooks with an
362 attached filament, would be reduced in mutants with a defective substrate specificity
363 switch. The distribution of attached filaments in the G183A mutant was similar to the WT
364 distribution (**Fig. S4**), however overall percentage of hooks with attached filaments has
365 decreased from 59% in the WT to 50% in G183A (**Fig. 3C**). Even though the R177H
366 mutant did not have a defect in HBB assembly, the ratio of hooks with attached filaments
367 was reduced to 38% in the mutant strain. In the ATPase activity mutants E211D and
368 E211Q, the maximum number of filaments per cell was reduced to four and two,
369 respectively. Consequently, the percentage of hooks with attached filaments decreased
370 to 25% and 11%, respectively. Nonetheless, both mutants (E211D, E211Q) showed
371 filament formation to some extent, whereas no filaments were detected in E215Q,
372 independent from the number of assembled HBBs. In summary, the reduction of hooks
373 with attached filaments in the FliI mutant strains support a defective substrate specificity
374 switch.

375 To further confirm the involvement of the FliI ATPase in the substrate specificity switch,
376 we measured the hook lengths of the WT and R177H and G183A mutants (**Fig. 3D-E**).
377 We hypothesized that the delayed substrate specificity switch in the mutants would
378 prolong the operating time of the T3SS in its early substrate secretion mode, resulting in
379 elongated hooks. Therefore, we purified HBB complexes from the WT, and R177H and
380 G183A mutants and measured the lengths of the hooks. Importantly, the lengths of the
381 hooks of both mutants were slightly increased. The WT displayed hooks with an average
382 length of 54.4 nm, whereas the hooks of the R177H mutant were on average 57.1 nm. In
383 line with the increased secretion of early substrates (**Fig. 2C**) in the G183A mutant, the
384 hooks from this mutant were even longer, on average 58.5 nm. The elongated hooks
385 assembled by the FliI mutants further confirm an involvement of the fT3SS ATPase FliI in
386 the substrate specificity switch.
387 Collectively, our results demonstrate that FliI couples ATPase activity to substrate
388 specificity switching of the fT3SS. The introduced point mutations impaired the transition
389 to late substrate secretion, as reflected in reduced class 3 gene expression, fewer hooks
390 with attached filaments, and elongated hooks. These effects are not due to defects in FliI
391 oligomerization or basal body localization, as confirmed by *in vivo* photo-crosslinking and
392 fluorescence microscopy. Thus, while FliI ATPase activity is dispensable for early
393 substrate secretion, it is important for efficient progression to the late assembly mode.

394 ## **Discussion**:

395 ATP hydrolysis by the FliI ATPase is essential for efficient operation of the fT3SS, but its
396 precise contribution to the temporal regulation of flagellar assembly has remained
397 unclear. In this study, we show that FliI activity is dispensable for early substrate secretion
398 but critically required for the substrate specificity switch and efficient export of late
399 substrates. The observed defect in the secretion of late substrates was not limited to FliC,
400 as secretion of other late substrates (FlgM, FlgK, FliD) was similarly impaired (**Fig. S2C**),
401 supporting a general role of FliI in facilitating late substrate export. Our analysis of FliI
402 point mutants demonstrates that they exhibit impaired late-stage assembly, with active
403 early substrate export and HBB formation, revealing a role for FliI in supporting the
404 transition to late secretion.

Table 1. Characteristics of the analyzed FliI mutants

	Relative motility	Relative early substrate secretion	Relative FliC-HiBiT secretion	Relative class 3 gene expression T_{90}	Hooks per cell	Hooks with attached filament [%]	Hook length [nm]
WT	1.00	1.00	1.000	1.000	3.1	58.7	54.4
Δ*fliI*	0.04	0.02	0.001	0.017	NA	NA	NA
R177H	0.48	1.00	0.417	0.183	3.1	38.2	57.1
G183A	0.93	1.38	0.754	0.778	3.0	50.5	58.5
E211D	0.25	0.62	0.135	0.034	2.6	24.9	NA
E211Q	0.09	0.37	0.003	0.027	0.5	11.4	NA
E215Q	0.06	0.13	0.001	0.022	0.1	0.0	NA

405

406 The key findings are summarized in **Table 1**. Notably, mutants such as R177H and
407 G183A, despite retaining early secretion and WT numbers of HBBs, exhibited strong

408 defects in late substrate secretion and reduced gene expression from class 3 promoters.
409 Mutants with impaired ATPase activity (E211D, E211Q, E215Q) showed progressively
410 more severe defects in all late assembly metrics. Importantly, these defects were not due
411 to loss of FliI oligomerization or localization, as demonstrated by *in vivo* photo-crosslinking
412 and fluorescence microscopy. Together, our data suggest that the function of the ATPase
413 activity of FliI is not merely to contribute to protein translocation but also facilitates the
414 transition of the fT3SS to late substrate export.
415 Recent structural and functional studies have proposed that FliHI modulate FlhA
416 conformation to stabilize the late export state (47). Our findings are fully consistent with
417 this model. It is likely that reduced ATPase activity or altered protein-protein interfaces in
418 our mutants impair this remodeling function, thereby disrupting efficient switching to late
419 substrate export. Additionally, we cannot exclude that FliI activity may contribute to
420 dissociation of late chaperone-substrate complexes, as shown for the ATPase InvC of the
421 evolutionary related virulence associated T3SS - processes that may be more ATP-
422 dependent than early substrate export (26).
423 Taken together, our findings support a model in which FliI performs multiple, coordinated
424 functions during flagellar assembly. First, FliI acts as a dynamic substrate carrier,
425 delivering substrates to the export gate (24). Second, it serves as an energy-coupling
426 ATPase that facilitates the efficient translocation of substrates through the fT3SS (27).
427 Third, FliI plays an active role in controlling the substrate specificity switch, likely by
428 modulating the conformational state of the export gate and promoting the transition from
429 early to late substrate export (47). Hence, rather than serving solely as an energy-
430 coupling translocase, FliI operates as a multi-functional ATPase that integrates substrate

431 delivery, energy coupling, and specificity switching, underscoring its central role in
432 flagellar biogenesis.

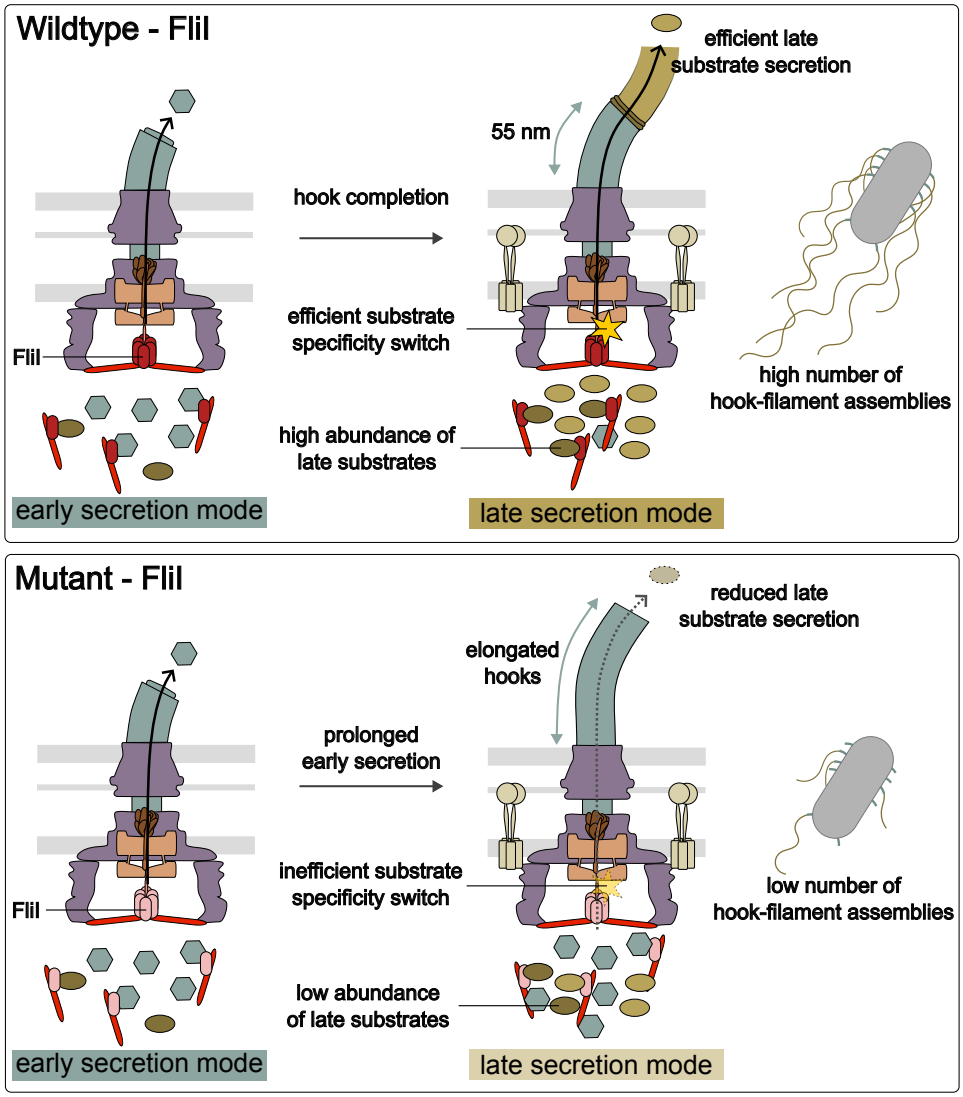

433

434 **Fig. 4** Schematic model of FliI function in wildtype and mutant strains. In wildtype cells (top), FliI facilitates
435 the transition from early to late secretion upon hook completion. This enables efficient FlgM secretion, timely
436 induction of class 3 gene expression, and robust export of late substrates, resulting in many hooks with
437 attached filaments. In FliI mutants (bottom), prolonged early secretion, delayed FlgM export, impaired class
438 3 gene expression, and inefficient late substrate export are observed. Consequently, hooks are elongated,
439 and fewer filaments are assembled.

440 ## Materials and Methods:

441 **Bacterial strains, plasmids and media**

442 All bacterial strains and plasmids used in this study are listed in Table S1 and were
443 derived from *S. enterica* subsp. *enterica* serovar Typhimurium LT2. Cells were cultivated
444 at 37 °C under aerobic conditions in lysogeny broth (LB) at 180 rpm. If not stated
445 otherwise, main cultures were diluted 1:100 and grown to mid-exponential phase. If
446 required, cultures were supplemented with ampicillin (cf = 100 µg/mL), chloramphenicol
447 (cf = 12.5 or 10 µg/mL) and/or AnTc (cf = 100 ng/mL). The FliI point mutations were
448 introduced chromosomally by site-specific mutagenesis using λ-Red homologous
449 recombination (48). Oligonucleotides used in this study are listed in Table S2.
450 Furthermore, the generalized transducing phage of *Salmonella enterica* serovar
451 Typhimurium P22 HT105/1 int-201 was used (49). Plasmids were constructed using
452 NEBuilder® HiFi DNA Assembly Master Mix (New England Biolabs, catalogue number
453 E2621L) ore one-step mutagenesis (50).

454

455 **Swimming motility assay**

456 Swimming motility was studied using tryptone broth-based soft agar swim plates
457 containing 0.3% Bacto agar. Motility plates were inoculated with 2 µL of overnight culture
458 and incubated at 37 °C for 4-5 h. Images were acquired by scanning the plates and the
459 diameters of the swimming halos were measured using Fiji (51). The swimming diameters
460 of the mutant strains were normalized to those of the WT.

461

462 **Subcellular localization of FliI**

463 The strains carried translational fusions of *fliG* to mNeonGreen and of HaloTag to *fliI*.
464 Additionally, the strains carried an AnTc inducible P_{tetA} promoter for the flagellar master
465 regulator operon *flhDC* (32). Overnight cultures were grown in 2 mL LB. Cultures were
466 diluted 1:100 in 10 mL of fresh LB and incubated at 37 °C for 1.5 h. The expression of
467 *flhDC* was induced by the addition of AnTc (cf = 100 ng/µL), followed by 1 h incubation at
468 37 °C. A 500 µL sample of each culture was collected and centrifuged at 2,550 × g for 3
469 min. Pellets were resuspended in 1 × PBS and adjusted to an OD_{600} of 0.3. A 150 µL
470 sample of each strain was transferred to a fresh 1.5 mL reaction tube and HaloTag
471 labeling was performed by adding the HaloTag ligand tetramethylrhodamine (cf = 0.5 µM,
472 Promega, catalogue number G8251) and incubating the samples for 30 min at 37 °C.
473 Cells were washed twice with 500 µL of 1 × PBS and resuspended in 300 µL of 1 × PBS
474 for microscopy. For imaging, 1 µL of labeled cells was spotted onto a 1% agarose pad in
475 1 × PBS. The cell suspension spot was air-dried for approximately 1 min and plasma-
476 cleaned glass coverslips were applied. Fluorescence microscopy was performed using a
477 Ti-2 Nikon inverted microscope equipped with a CFI Plan Apochromat DM 60× Lambda
478 oil Ph3/1.40 (Nikon) oil objective, an Orca Fusion BT camera (Hamamatsu), and a
479 SPECTRA III LED light source (Lumencor). Z-stacks were acquired in a 1.6 µm range
480 with 5 stacks at 0.4 µm intervals. Microscopy data was analyzed using a custom Jupyter
481 Notebook (See data and code availability statement) and Ilastik v1.4.0 (52).

482

483 ***In vivo* photo-crosslinking of the FliI hexamer**

484 The protocol for *in vivo* photo-crosslinking to study the ability of FliI to form hexamers was
485 adapted from previously published protocols (53, 54). Strains were deleted for *fliI*, carried
486 pSUP and expressed $FliI_{3\times FLAG}$ (with amber mutation and respective point mutations)
487 constitutively from pTrc99A-FF4. Overnight cultures were grown in LB, supplemented
488 with chloramphenicol (cf = 10 µg/mL) and ampicillin (cf = 100 µg/mL) at 37 °C, 180 rpm.
489 Main cultures were diluted 1:100 in 10 mL LB with the respective supplements in the
490 presence of 1 mM *p*Bpa at 37 °C until they reached mid-exponential phase. 9 mL of each
491 culture was harvested at 4,000 × g, 4 °C for 5 min. Cells were washed once with 2 mL
492 cold 1 × PBS and pelleted again with centrifugation. Cells were resuspended in 2 mL cold
493 1 × PBS. 1 mL of the cell culture was transferred into a fresh 1.5 mL reaction tube; another
494 1 mL was transferred into a 6-well cell culture dish and irradiated for 30 min with UV light
495 (λ = 366 nm) on ice. Afterwards, the cells were transferred into a fresh 1.5 mL reaction
496 tube harvested at 10,000 × g at 4 °C for 3 min. Proteins were precipitated using 10% (v/v)
497 TCA, followed by 30 min incubation on ice. Proteins were pelleted by centrifugation at
498 20,000 × g for 30 min at 4 °C. Protein pellets were washed with ice-cold acetone and air-
499 dried. Samples were adjusted to 50 OD units/µL. 500 OD units were analyzed under
500 denaturing conditions using SDS-PAGE. Immunoblotting was performed using primary α-
501 FLAG antibody (Sigma-Aldrich, catalogue number F1804-200UG, 1:10,000 in 1 × TBS-
502 T). Proteins were detected using secondary α-mouse antibodies conjugated to
503 horseradish peroxidase (Bio-Rad Immun-Star Goat Anti-Mouse (GAM)-HRP Conjugate,
504 catalog number 170-5047, 1:20,000 in 1 × TBS-T).

505

506 **Minimal inhibitory concentration assay (FlgE-Bla secretion)**

507 The minimal inhibitory concentration (MIC) of ampicillin correlating with the amount of
508 secreted hook-protein-β-lactamase fusion protein (FlgE-Bla) was determined as
509 described by Lee et al. (36) and adapted by Singer et al. (37) to fit a 96-well plate format.
510 Briefly, cultures were grown overnight in 200 µL LB in a 96-well plate at 37 °C, 180 rpm
511 in biological triplicates. The cultures were diluted 1:100 in fresh LB and grown to mid-
512 exponential phase at 37 °C at 180 rpm. The cultures were then diluted 1:10 in 300 µL LB
513 and finally diluted 1:10 in 200 µL LB media supplemented with increasing concentrations
514 of fresh ampicillin (Amp) in technical triplicates. Cells were grown for 4.5 h at 37 °C at
515 180 rpm and OD_{600} was measured with a microplate reader. The IC_{50} was calculated
516 using a custom Jupyter Notebook.

517

518 **Secretion Assay using the split NanoBit® enzyme**

519 Nano-Glo® HiBiT Extracellular Detection System was purchased from Promega (N2420).
520 Quantification of the secreted HiBiT-tagged proteins was determined as described
521 previously (41). Briefly, overnight cultures were diluted 1:100 and grown to late
522 exponential phase at 37 °C at 180 rpm. OD_{600} was measured and 1 mL sample of each
523 culture was transferred into a 1.5 mL Eppendorf tube on ice. Samples were centrifuged
524 at 13,000 x g at 4 °C for 3 min. 500 µL of the supernatant (SN) was transferred into a
525 fresh Eppendorf tube and stored on ice. 25 µL of the SN was transferred in technical
526 triplicates into a white 384-well plate with LB-blanks included. The working solution was
527 prepared and SN samples and working solution were mixed as described by the
528 manufacturer. Luminescence was measured at T_0 = 0 min and T_{10} = 10 min using a

529 microplate reader. The relative light units (RLU) of each strain were calculated using
530 following equation:

531 $$RLU = (t_{10} - t_0) - (mean\ of\ blank)$$

532 The calculated values were normalized to the measured OD_{600} and to the WT strain.

533

534 **Secretion Assay analyzed by SDS-PAGE and Western Blot**

535 For analysis with SDS-PAGE and Western Blotting, the same cultures were used as for
536 the secretion assay using the split luciferase. A 1.9 mL aliquot was taken, and cells were
537 harvested by centrifugation at 13,000 × g for 5 min. 1 mL of the supernatant was
538 transferred into a fresh tube, the remaining supernatant was discarded, and the cell
539 pellets were resuspended in 1 mL of double-distilled water. Proteins were precipitated
540 using 10% (v/v) TCA, followed by 30 min incubation on ice. Proteins were pelleted by
541 centrifugation at 20,000 × g for 30 min at 4 °C. Protein pellets were washed with ice-cold
542 acetone and air-dried. Samples were adjusted to 20 OD units/µL. 200 OD units were
543 analyzed under denaturing conditions using SDS-PAGE. The samples of all three
544 biological replicates were pooled to obtain the mean protein amount of all replicates.
545 Immunoblotting was performed using primary α-FlgM (gift from K. Hughes, 1:10,000 in
546 1 × TBS-T), α-FlgK (gift from T. Minamino, 1:10,000 in 1 × TBS-T), α-FliD (gift from T.
547 Minamino, 1:10,000 in 1 × TBS-T) or α-FliC (Difco, catalog number 228241 Salmonella H
548 Antiserum I, 1:5,000 in 1 × TBS-T) antibodies. Proteins were detected using secondary
549 α-rabbit antibodies conjugated to horseradish peroxidase (Bio-Rad Immun-Star Goat
550 Anti-Rabbit (GAR)-HRP Conjugate, catalog number 170-5046, 1:20,000 in 1 × TBS-T).
551 The relative amounts of secreted and cellular proteins were determined by normalization

552 to the housekeeping protein DnaK using the Image Lab software (Bio-Rad). DnaK was
553 detected using a primary α-DnaK (abcam, catalog number ab69617, 1:10,000 in 1 × TBS-
554 T) antibody and secondary α-mouse antibodies conjugated to horseradish peroxidase
555 (Bio-Rad Immun-Star Goat Anti-Mouse (GAM)-HRP Conjugate, catalog number 170-
556 5047, 1:20,000 in 1 × TBS-T).
557
558 **Luciferase assay – P_{motA}-*luxCDABE***
559 Strains harboring the plasmid pRG19 (P_{motA}-*luxCDABE*) were used to monitor flagellar
560 class 3 gene expression (44). ON-cultures of 6 biological replicates were grown in 200 µL
561 LB supplemented with Chloramphenicol (Cm) with cf = 12.5 µg/ml in a 96-well plate at 37
562 °C, 200 rpm. To prevent evaporation, the plate was covered with a Breath-Easy sealing
563 membrane. The cultures were diluted 1:10 in 200 µL LB supplemented with Cm and again
564 1:10 in LB supplemented with Cm and AnTc to a final concentration of 100 ng/ml to induce
565 expression of the flagellar master regulator from P_{tetA} (32) in a white 96-well plate for final
566 dilution to 1:100. The OD_{600} was measured, as well as luminescence with a microplate
567 reader for 6 h every 15 min. The relative light units (RLU) were normalized to the
568 measured OD_{600} of each sample and analyzed as described previously (45, 55). The
569 relative class 3 gene expression in respect to the WT was calculated for three timepoints
570 T_{360} (360 min).
571
572 **Hook and Filament Staining**
573 For determination of the number of hooks per cell and the number of hooks with an
574 attached filament, cells were grown to mid-log phase. 500 µL samples were taken and

575 centrifuged at 2500 × g for 5 min. The cells were carefully resuspended in 500 μL fresh 1
576 × PBS. Star Green maleimide dye (Abberior, catalogue number STGREEN-0003-1MG)
577 with cf = 10 μM and 0.5 μL α-HA-Alexa555 (Thermo Fisher Scientific, catalogue number
578 26183-A555) were added to stain the filaments (*fliC*$_{T237C}$) (56) with maleimide and the
579 hook (*flgE*$_{3\times HA}$) with immunostaining. The cells were incubated for 1 h at 37 °C at 300
580 rpm. The cells were washed twice with 1 × PBS before loading the samples on a poly-L-
581 lysine coated coverslip as described previously (57, 58). The cells were fixed using 2%
582 paraformaldehyde-0.2% glutaraldehyde solution and rinsed with 1 × PBS before staining
583 the DNA fluoroshield containing DAPI (Sigma Aldrich, catalogue number F6057-20ML).
584 Cells were observed using a Zeiss Inverted Microscope Axio Observer Z1 at 100 ×
585 magnification and z-stack experiments were performed with 9 slices, 4 μm range with 0.5
586 μm slice interval. Analysis was done using Fiji for image processing equipped with the
587 MicrobeJ Plugin to determine the number of hooks per cell (51, 59). Filaments were
588 counted manually on cells with determined hook numbers.
589

590 **Hook Length Measurements**

591 The purification of hook basal body complexes was adapted from a previously published
592 protocol (6, 12, 60). Briefly, an overnight culture was inoculated with a single colony in LB
593 medium. The next day, 500 mL LB medium was inoculated 1:100 with the overnight
594 culture and grown for 2.5 h. We utilized strains with an AnTc inducible P_{tetA} promoter for
595 the flagellar master regulator operon *flhDC* (32). To induce flagella biosynthesis, AnTc
596 was added, and the cells were further inoculated for 1 h. Cells were harvested at
597 4,000 × g at 4 °C for 15 min. The cell pellet was carefully resuspended in 20 mL ice-cold

598 sucrose solution (0.5 M sucrose, 0.15 M Trizma base, unaltered pH) on ice. Lysozyme
599 and EDTA pH 4.7 were added slowly to final concentrations of 0.1 mg/mL and 2 mM,
600 respectively, while stirring the cell suspension on ice. After 5 min of stirring on ice, the
601 suspension was transferred to RT and slowly stirred for 1 h to allow spheroplast formation.
602 For cell lysis, Triton X-100 was added to a final concentration of 1%. After rapidly stirring
603 the suspension for 10 min until it became translucent, it was slowly stirred further for 30-
604 45 min on ice. To degrade DNA, 2 mg DNAseI and $MgSO_4$ were added to a final
605 concentration of 5 mM while stirring on ice. After 5 min, EDTA pH 4.7 was added at a final
606 concentration of 5 mM. To pellet cell debris and unlysed cells, the suspension was
607 centrifuged at 15,000 × g at 4 °C for 10 min. The supernatant was collected and
608 centrifuged at 37,000 rpm (T-647.5 Fixed Angle Rotor, Thermo Fisher Scientific) for 1 h
609 at 4 °C to pellet the flagella. The flagella were washed carefully with 50 mL buffer A (0.1
610 M KCl, 0.3 M sucrose, 0.1% Triton X-100) and collected again at 37,000 rpm (T-647.5
611 Fixed Angle Rotor, Thermo Fisher Scientific) for 1 h at 4 °C. To depolymerize the flagellin
612 filament, the pellet was carefully resuspended in 50 mL buffer B (50 mM glycine, 0.1%
613 Triton X-100, pH 2.5), followed by 30 min incubation at room temperature. Finally, the
614 hook basal bodies were collected again by centrifugation at 37,000 rpm (T-647.5 Fixed
615 Angle Rotor, Thermo Fisher Scientific) for 1 h at 4 °C. Hook basal bodies were
616 resuspended carefully in 50 µL buffer C (10 mM Tris pH 8, 5 mM EDTA pH 8, 0.1% Triton
617 X-100) and incubated overnight on a rolling platform at 4 °C. Grids were prepared as
618 described previously (61). Briefly, aliquots of HBB samples were applied to freshly glow
619 discharged carbon-film-coated copper grids and allowed to adsorb for 10 minutes. After
620 three washes with distilled water, the grids were contrasted with 4% phospho-tungstic-

621 acid/1% trehalose, touched on filter paper and air-dried. The grids were analyzed in a Leo
622 906 transmission electron microscope (Zeiss) at 100 kV acceleration voltage.
623 Micrographs were scanned using a Morada side-mount camera (SIS) with ImageSP
624 software from TRS (Tröndle). Hook lengths were measured using Fiji (51).
625

626 **Statistical Analyses**

627 Statistical analyses were performed using GraphPad Prism 10 (GraphPad Software), and
628 values of $P < 0.05$ were considered statistically significant.
629

630 **Data and code availability**

631 The Jupyter notebook used for colocalization analyses of the microscopy data is available
632 at **https://github.com/SalmoLab/FliI_ATPase**.

Acknowledgements:

M.E. acknowledges funding from the Deutsche Forschungsgemeinschaft (DFG) research grant no. 322866343 and from the Max Planck Society as Max Planck Fellow. M.D.G. was supported by a Grand Challenge Initiative Global Health grant of the Berlin University Alliance (no.113_MC_GH_MEL-BER_Erhardt_HU). We thank K. Hughes (The University of Utah) and T. Minamino (Osaka University) for providing antibodies. We thank members of the Erhardt lab for helpful discussions and critical comments on the manuscript, and Heidi Landmesser and Raúl Trepel-Washington for technical assistance.

641 **Author Contributions:**

642 M.E. conceptualized and supervised the research project and ensured funding. R.E. and
643 M.D.G. generated *S. enterica* mutants. R.E. performed the experiments, wrote the first
644 draft of the manuscript and prepared figures. L.H. wrote the code for colocalization
645 analyses for the microscopy data. C.G. prepared TEM grids and observed the purified
646 HBB samples. M.E. reviewed and edited the manuscript. All authors reviewed the results
647 and approved the final version of the manuscript.

648 **References:**

649 1. Berg, HC, Anderson, RA. 1973. Bacteria Swim by Rotating their Flagellar Filaments.
650 Nature 245:380–382.

651 2. Horstmann, JA, Lunelli, M, Cazzola, H, Heidemann, J, Kühne, C, Steffen, P, Szefs,
652 S, Rossi, C, Lokareddy, RK, Wang, C, Lemaire, L, Hughes, KT, Uetrecht, C,
653 Schlüter, H, Grassl, GA, Stradal, TEB, Rossez, Y, Kolbe, M, Erhardt, M. 2020.
654 Methylation of *Salmonella* Typhimurium flagella promotes bacterial adhesion and
655 host cell invasion. Nat. Commun. 11:2013.

656 3. Tan, J, Zhang, X, Wang, X, Xu, C, Chang, S, Wu, H, Wang, T, Liang, H, Gao, H,
657 Zhou, Y, Zhu, Y. 2021. Structural basis of assembly and torque transmission of the
658 bacterial flagellar motor. Cell 184:2665–2679.e19.

659 4. Johnson, S, Furlong, EJ, Deme, JC, Nord, AL, Caesar, JJE, Chevance, FFV, Berry,
660 RM, Hughes, KT, Lea, SM. 2021. Molecular structure of the intact bacterial flagellar
661 basal body. Nat. Microbiol. 6:712–721.

662 5. Singh, PK, Sharma, P, Afanzar, O, Goldfarb, MH, Maklashina, E, Eisenbach, M,
663 Cecchini, G, Iverson, TM. 2024. CryoEM structures reveal how the bacterial
664 flagellum rotates and switches direction. Nat. Microbiol. 9:1271–1281.

665 6. Johnson, S, Deme, JC, Furlong, EJ, Caesar, JJE, Chevance, FFV, Hughes, KT, Lea,
666 SM. 2024. Structural basis of directional switching by the bacterial flagellum. Nat.
667 Microbiol.

668 7. Tan, J, Zhang, L, Zhou, X, Han, S, Zhou, Y, Zhu, Y. 2024. Structural basis of the
669 bacterial flagellar motor rotational switching. Cell Res. 34:788–801.

670 8. Santiveri, M, Roa-Eguiara, A, Kühne, C, Wadhwa, N, Hu, H, Berg, HC, Erhardt, M,
671 Taylor, NMI. 2020. Structure and Function of Stator Units of the Bacterial Flagellar
672 Motor. Cell 183:244–257.e16.

673 9. Kato, T, Makino, F, Miyata, T, Horváth, P, Namba, K. 2019. Structure of the native
674 supercoiled flagellar hook as a universal joint. Nat. Commun. 10:5295.

675 10. Spöring, I, Martinez, VA, Hotz, C, Schwarz-Linek, J, Grady, KL, Nava-Sedeño, JM,
676 Vissers, T, Singer, HM, Rohde, M, Bourquin, C, Hatzikirou, H, Poon, WCK, Dufour,
677 YS, Erhardt, M. 2018. Hook length of the bacterial flagellum is optimized for maximal
678 stability of the flagellar bundle. PLoS Biol. 16:e2006989.

679 11. Erhardt, M, Singer, HM, Wee, DH, Keener, JP, Hughes, KT. 2011. An infrequent
680 molecular ruler controls flagellar hook length in *Salmonella enterica*. EMBO J.
681 30:2948–2961.

682 12. Einenkel, R, Qin, K, Schmidt, J, Al-Otaibi, NS, Mann, D, Drobnič, T, Cohen, EJ,
683 Gonzalez-Rodriguez, N, Harrowell, J, Shmakova, E, Beeby, M, Erhardt, M,
684 Bergeron, JRC. 2025. The structure of the complete extracellular bacterial flagellum
685 reveals the mechanism of flagellin incorporation. Nat. Microbiol.

686 13. Al-Otaibi, NS, Taylor, AJ, Farrell, DP, Tzokov, SB, DiMaio, F, Kelly, DJ, Bergeron,
687 JRC. 2020. The cryo-EM structure of the bacterial flagellum cap complex suggests
688 a molecular mechanism for filament elongation. Nat. Commun. 11:3210.

689 14. Erhardt, M, Mertens, ME, Fabiani, FD, Hughes, KT. 2014. ATPase-Independent
690 Type-III Protein Secretion in *Salmonella enterica*. PLoS Genet. 10:e1004800.

691 15. Halte, M, Erhardt, M. 2021. Protein Export via the Type III Secretion System of the
692 Bacterial Flagellum. Biomolecules 11

693 16. Chen, S, Beeby, M, Murphy, GE, Leadbetter, JR, Hendrixson, DR, Briegel, A, Li, Z,
694 Shi, J, Tocheva, EI, Müller, A, Dobro, MJ, Jensen, GJ. 2011. Structural diversity of
695 bacterial flagellar motors. EMBO J. 30:2972–2981.

696 17. Claret, L, Calder, SR, Higgins, M, Hughes, C. 2003. Oligomerization and activation
697 of the FliI ATPase central to bacterial flagellum assembly. Mol. Microbiol. 48:1349–
698 1355.

699 18. Ibuki, T, Imada, K, Minamino, T, Kato, T, Miyata, T, Namba, K. 2011. Common
700 architecture of the flagellar type III protein export apparatus and F- and V-type
701 ATPases. Nat. Struct. Mol. Biol. 18:277–282.

702 19. Imada, K, Minamino, T, Tahara, A, Namba, K. 2007. Structural similarity between
703 the flagellar type III ATPase FliI and F1-ATPase subunits. Proc. Natl. Acad. Sci.
704 U.S.A. 104:485–490.

705 20. Imada, K, Minamino, T, Uchida, Y, Kinoshita, M, Namba, K. 2016. Insight into the
706 flagella type III export revealed by the complex structure of the type III ATPase and
707 its regulator. Proc. Natl. Acad. Sci. U.S.A. 113:3633–3638.

708 21. Minamino, T, Yoshimura, SDJ, Morimoto, YV, González-Pedrajo, B, Kami-ike, N,
709 Namba, K. 2009. Roles of the extreme N-terminal region of FliH for efficient
710 localization of the FliH–FliI complex to the bacterial flagellar type III export
711 apparatus. Mol. Microbiol. 74:1471–1483.

712 22. Minamino, T, Morimoto, YV, Hara, N, Namba, K. 2011. An energy transduction
713 mechanism used in bacterial flagellar type III protein export. Nat. Commun. 2:475.

714 23. Trampari, E, Stevenson, CE, Little, RH, Wilhelm, T, Lawson, DM, Malone, JG. 2015.
715 Bacterial rotary export ATPases are allosterically regulated by the nucleotide second
716 messenger cyclic-di-GMP. J. Biol. Chem. 290:24470–24483.

717 24. Bai, F, Morimoto, YV, Yoshimura, SDJ, Hara, N, Kami-ike, N, Namba, K, Minamino,
718 T. 2014. Assembly dynamics and the roles of FliI ATPase of the bacterial flagellar
719 export apparatus. Sci. Rep. 4:6528.

720 25. Kucera, J, Terentjev, EM. 2020. $FliI_6$-FliJ molecular motor assists with unfolding in
721 the type III secretion export apparatus. Sci. Rep. 10:7127.

722 26. Akeda, Y, Galán, JE. 2005. Chaperone release and unfolding of substrates in type
723 III secretion. Nature 437:911–915.

724 27. Minamino, T, Kinoshita, M, Namba, K. 2022. Insight Into Distinct Functional Roles
725 of the Flagellar ATPase Complex for Flagellar Assembly in *Salmonella*. Front.
726 Microbiol. 13

727 28. Gillen, KL, Hughes, KT. 1991. Molecular characterization of *flgM*, a gene encoding
728 a negative regulator of flagellin synthesis in *Salmonella typhimurium*. J. Bacteriol.
729 173:6453–6459.

730 29. Hughes, KT, Gillen, KL, Semon, MJ, Karlinsey, JE. 1993. Sensing Structural
731 Intermediates in Bacterial Flagellar Assembly by Export of a Negative Regulator.
732 Science 262:1277–1280.

733 30. Chevance, FF, Hughes, KT. 2008. Coordinating assembly of a bacterial
734 macromolecular machine. Nat. Rev. Microbiol. 6:455–465.

735 31. Minamino, T, Morimoto, YV, Kinoshita, M, Aldridge, PD, Namba, K. 2014. The
736 bacterial flagellar protein export apparatus processively transports flagellar proteins
737 even with extremely infrequent ATP hydrolysis. Sci. Rep. 4:7579.

738 32. Karlinsey, JE, Tanaka, S, Bettenworth, V, Yamaguchi, S, Boos, W, Aizawa, S-I,
739 Hughes, KT. 2000. Completion of the hook–basal body complex of the *Salmonella*
740 *typhimurium* flagellum is coupled to FlgM secretion and *fliC* transcription. Mol.
741 Microbiol. 37:1220–1231.

742 33. Minamino, T, Kazetani, K-i, Tahara, A, Suzuki, H, Furukawa, Y, Kihara, M, Namba,
743 K. 2006. Oligomerization of the Bacterial Flagellar ATPase FliI is Controlled by its
744 Extreme N-terminal Region. J. Mol. Biol. 360:510–519.

745 34. Okabe, M, Minamino, T, Imada, K, Namba, K, Kihara, M. 2009. Role of the N-
746 terminal domain of FliI ATPase in bacterial flagellar protein export. FEBS Lett.
747 583:743–748.

748 35. Minamino, T, Inoue, Y, Kinoshita, M, Namba, K. 2020. FliK-Driven Conformational
749 Rearrangements of FlhA and FlhB Are Required for Export Switching of the Flagellar
750 Protein Export Apparatus. J. Bacteriol. 202

751 36. Lee, HJ, Hughes, KT. 2006. Posttranscriptional control of the *Salmonella enterica*
752 flagellar hook protein FlgE. J. Bacteriol. 188:3308–3316.

753 37. Singer, HM, Erhardt, M, Hughes, KT. 2014. Comparative analysis of the secretion
754 capability of early and late flagellar type III secretion substrates. Mol. Microbiol.
755 93:505–520.

756 38. Minamino, T, Macnab, R. 1999. Components of the *Salmonella* Flagellar Export
757 Apparatus and Classification of Export Substrates. J. Bacteriol. 181:1388–1394.

758 39. Dixon, AS, Schwinn, MK, Hall, MP, Zimmerman, K, Otto, P, Lubben, TH, Butler, BL,
759 Binkowski, BF, Machleidt, T, Kirkland, TA, Wood, MG, Eggers, CT, Encell, LP,
760 Wood, KV. 2016. NanoLuc Complementation Reporter Optimized for Accurate
761 Measurement of Protein Interactions in Cells. ACS Chem. Biol. 11:400–408.

762 40. Hall, MP, Unch, J, Binkowski, BF, Valley, MP, Butler, BL, Wood, MG, Otto, P,
763 Zimmerman, K, Vidugiris, G, Machleidt, T, Robers, MB, Benink, HA, Eggers, CT,
764 Slater, MR, Meisenheimer, PL, Klaubert, DH, Fan, F, Encell, LP, Wood, KV. 2012.
765 Engineered Luciferase Reporter from a Deep Sea Shrimp Utilizing a Novel
766 Imidazopyrazinone Substrate. ACS Chem. Biol. 7:1848–1857.

767 41. Einenkel, R, Halte, M, Erhardt, M. *In* Journet, L, Cascales, E (ed), Quantifying
768 Substrate Protein Secretion via the Type III Secretion System of the Bacterial
769 Flagellum Bacterial Secretion Systems, p. 577–592. Bacterial Secretion Systems:
770 Methods and Protocols, Humana, New York, NY.

771 42. Ohnishi, K, Kutsukake, K, Suzuki, H, Lino, T. 1992. A novel transcriptional regulation
772 mechanism in the flagellar regulon of *Salmonella typhimurium*: an anti-sigma factor
773 inhibits the activity of the flagellum-specific Sigma factor, σF. Mol. Microbiol. 6:3149–
774 3157.

775 43. Chadsey, MS, Karlinsey, JE, Hughes, KT. 1998. The flagellar anti-σ factor FlgM
776 actively dissociates *Salmonella typhimurium* σ28 RNA polymerase holoenzyme.
777 Genes Dev. 12:3123–3136.

778 44. Goodier, RI, Ahmer, BM. 2001. SirA orthologs affect both motility and virulence. J.
779 Bacteriol. 183:2249–2258.

780 45. Erhardt, M, Hirano, T, Su, Y, Paul, K, Wee, DH, Mizuno, S, Aizawa, S, Hughes, KT.
781 2010. The role of the FliK molecular ruler in hook-length control in *Salmonella*
782 *enterica*. Mol. Microbiol. 75:1272–1284.

783 46. Moriya, N, Minamino, T, Hughes, KT, Macnab, RM, Namba, K. 2006. The Type III
784 Flagellar Export Specificity Switch is Dependent on FliK Ruler and a Molecular
785 Clock. J. Mol. Biol. 359:466–477.

786 47. Kinoshita, M, Minamino, T, Uchihashi, T, Namba, K. 2024. FliH and FliI help FlhA
787 bring strict order to flagellar protein export in *Salmonella*. Commun. Biol. 7:366.

788 48. Blank, K, Hensel, M, Gerlach, RG. 2011. Rapid and Highly Efficient Method for
789 Scarless Mutagenesis within the *Salmonella enterica* Chromosome. PLoS One
790 6:e15763.

791 49. Sanderson, KE, Roth, JR. 1983. Linkage map of *Salmonella typhimurium*, Edition
792 VI. Microbiol. Rev. 47:410–453.

793 50. Liu, H, Naismith, JH. 2008. An efficient one-step site-directed deletion, insertion,
794 single and multiple-site plasmid mutagenesis protocol. An efficient one-step site-
795 directed deletion, insertion, single and multiple-site plasmid mutagenesis protocol
796 8:91.

797 51. Schindelin, J, Arganda-Carreras, I, Frise, E, Kaynig, V, Longair, M, Pietzsch, T,
798 Preibisch, S, Rueden, C, Saalfeld, S, Schmid, B, Tinevez, J-Y, White, DJ,
799 Hartenstein, V, Eliceiri, K, Tomancak, P, Cardona, A. 2012. Fiji: an open-source
800 platform for biological-image analysis. Nat. Methods 9:676–682.

801 52. Berg, S, Kutra, D, Kroeger, T, Straehle, CN, Kausler, BX, Haubold, C, Schiegg, M,
802 Ales, J, Beier, T, Rudy, M, Eren, K, Cervantes, JI, Xu, B, Beuttenmueller, F, Wolny,
803 A, Zhang, C, Koethe, U, Hamprecht, FA, Kreshuk, A. 2019. ilastik: interactive
804 machine learning for (bio)image analysis. Nat. Methods 16:1226–1232.

805 53. Dietsche, T, Tesfazgi Mebrhatu, M, Brunner, MJ, Abrusci, P, Yan, J, Franz-Wachtel,
806 M, Schärfe, C, Zilkenat, S, Grin, I, Galán, JE, Kohlbacher, O, Lea, S, Macek, B,
807 Marlovits, TC, Robinson, CV, Wagner, S. 2016. Structural and Functional
808 Characterization of the Bacterial Type III Secretion Export Apparatus. PLoS Pathog.
809 12:e1006071.

810 54. Miyazaki, R, Akiyama, Y, Mori, H. 2020. A photo-cross-linking approach to monitor
811 protein dynamics in living cells. BBA - Gen. Subj. 1864:129317.

812 55. Brown, JD, Saini, S, Aldridge, C, Herbert, J, Rao, CV, Aldridge, PD. 2008. The rate
813 of protein secretion dictates the temporal dynamics of flagellar gene expression.
814 Mol. Microbiol. 70:924–937.

815 56. Renault, TT, Abraham, AO, Bergmiller, T, Paradis, G, Rainville, S, Charpentier, E,
816 Guet, CC, Tu, Y, Namba, K, Keener, JP, Minamino, T, Erhardt, M. 2017. Bacterial
817 flagella grow through an injection-diffusion mechanism. eLife 6

818 57. Erhardt, M. 2017. Fluorescent Microscopy Techniques to Study Hook Length Control
819 and Flagella Formation. Methods Mol. Biol. 1593:37–46.

820 58. Wozniak, CE, Chevance, FF, Hughes, KT. 2010. Multiple promoters contribute to
821 swarming and the coordination of transcription with flagellar assembly in *Salmonella*.
822 J. Bacteriol. 192:4752–4762.

823 59. Ducret, A, Quardokus, EM, Brun, YV. 2016. MicrobeJ, a tool for high throughput
824 bacterial cell detection and quantitative analysis. Nat. Microbiol. 1:16077.

825 60. Francis, NR, Sosinsky, GE, Thomas, D, DeRosier, DJ. 1994. Isolation,
826 characterization and structure of bacterial flagellar motors containing the switch
827 complex. J. Mol. Biol. 235:1261–1270.

828 61. Halte, M, Andrianova, EP, Goosmann, C, Chevance, FFV, Hughes, KT, Zhulin, IB,
829 Erhardt, M. 2024. FlhE functions as a chaperone to prevent formation of periplasmic
830 flagella in Gram-negative bacteria. Nat. Commun. 15:5921.